40 W Continuous Wave Ce:Nd:YAG Solar Laser through a Fused Silica Light Guide

Joana Almeida, Dawei Liang, Dário Garcia, Bruno Tibúrcio, Hugo Costa, Miguel Catela, Emmanuel Guillot, Cláudia Vistas

▶ **To cite this version:**

Joana Almeida, Dawei Liang, Dário Garcia, Bruno Tibúrcio, Hugo Costa, et al.. 40 W Continuous Wave Ce:Nd:YAG Solar Laser through a Fused Silica Light Guide. Energies, 2022, 15 (11), pp.3998. ⟨10.3390/en15113998⟩. ⟨hal-04041741⟩

HAL Id: hal-04041741

https://hal.science/hal-04041741v1

Submitted on 8 Dec 2023

HAL is a multi-disciplinary open access archive for the deposit and dissemination of scientific research documents, whether they are published or not. The documents may come from teaching and research institutions in France or abroad, or from public or private research centers.

L'archive ouverte pluridisciplinaire **HAL**, est destinée au dépôt et à la diffusion de documents scientifiques de niveau recherche, publiés ou non, émanant des établissements d'enseignement et de recherche français ou étrangers, des laboratoires publics ou privés.

HAL Authorization

energies

MDPI

Article

40 W Continuous Wave Ce:Nd:YAG Solar Laser through a Fused Silica Light Guide

Joana Almeida [1], Dawei Liang [1,*], Dário Garcia [1], Bruno D. Tibúrcio [1], Hugo Costa [1], Miguel Catela [1], Emmanuel Guillot [2] and Cláudia R. Vistas [1]

[1] Centro de Física e Investigação Tecnológica (CEFITEC), Departamento de Física, Faculdade de Ciências e Tecnologia, Universidade NOVA de Lisboa, 2829-516 Caparica, Portugal; jla@fct.unl.pt (J.A.); dm.garcia@campus.fct.unl.pt (D.G.); brunotiburcio78@gmail.com (B.D.T.); hf.costa@campus.fct.unl.pt (H.C.); m.catela@campus.fct.unl.pt (M.C.); c.vistas@fct.unl.pt (C.R.V.)

[2] PROMES-CNRS, 7 rue du Four Solaire, 66120 Font-Romeu-Odeillo-Via, France; emmanuel.guillot@promes.cnrs.fr

* Correspondence: dl@fct.unl.pt

Abstract: The solar laser power scaling potential of a side-pumped Ce:Nd:YAG solar laser through a rectangular fused silica light guide was investigated by using a 2 m diameter parabolic concentrator. The laser head was formed by the light guide and a V-shaped pump cavity to efficiently couple and redistribute the concentrated solar radiation from the parabolic mirror to a 4 mm diameter, 35 mm length Ce(0.1 at.%):Nd(1.1 at.%):YAG laser rod. The rectangular light guide ensured a homogeneous distribution of the solar radiation along the laser rod, allowing it to withstand highly concentrated solar energy. With the full collection area of the parabolic mirror, the maximum continuous wave (cw) solar laser power of 40 W was measured. This, to the best of our knowledge, corresponds to the highest cw laser power obtained from a Ce:Nd:YAG medium pumped by solar radiation, representing an enhancement of two times over that of the previous side-pumped Ce:Nd:YAG solar laser and 1.19 times over the highest Cr:Nd:YAG solar laser power with a rectangular light-guide. This research proved that, with an appropriate pumping configuration, the Ce:Nd:YAG medium is very promising for scaling solar laser output power to a higher level.

Keywords: Ce:Nd:YAG; solar laser; light-guide; homogenizer; side-pumped; parabolic mirror

check for updates

Citation: Almeida, J.; Liang, D.; Garcia, D.; Tibúrcio, B.D.; Costa, H.; Catela, M.; Guillot, E.; Vistas, C.R. 40 W Continuous Wave Ce:Nd:YAG Solar Laser through a Fused Silica Light Guide. *Energies* **2022**, *15*, 3998. https://doi.org/10.3390/en15113998

Academic Editor: Albert Ratner

Received: 12 May 2022
Accepted: 27 May 2022
Published: 29 May 2022

Publisher's Note: MDPI stays neutral with regard to jurisdictional claims in published maps and institutional affiliations.

Copyright: © 2022 by the authors. Licensee MDPI, Basel, Switzerland. This article is an open access article distributed under the terms and conditions of the Creative Commons Attribution (CC BY) license (https://creativecommons.org/licenses/by/4.0/).

1. Introduction

Solar-powered laser systems directly convert broadband and incoherent solar radiation into narrowband and coherent laser radiation through an active medium. Since this technology can be operated using only renewable energy, it may bring an important economic advantage for countries with high solar availability [1] and for the future development of sustainable industrialization [2], either on Earth [3,4] or in Space [5,6].

The first laser emission achieved by pumping an active medium with solar energy was reported by Kiss et al. in 1963, based on a calcium fluoride crystal doped with a divalent dysprosium (Dy^{2+}:CaF_2) medium, reaching the continuous wave (cw) laser action at 2.36 μm [7]. Thenceforth, optical pumping designs and active media have been investigated for solar-pumped lasers. Between the late 1970s and early 2000s, gas [6,8,9], liquid [10], and solid [11–13] active media have all been evaluated as potential candidates for solar-pumped lasers. Still, this research has essentially converged in the use of bulk solid-state optical gain media, namely the yttrium aluminum garnet ($Y_3Al_5O_{12}$) doped with the rare earth ion neodymium (Nd^{3+}) [14–27]. The favorable spectroscopic characteristics of the Nd^{3+} active ion and optomechanical properties of the YAG host material [28], in conjunction with the advances in the optical pumping designs, have contributed to the progress of solar-pumped lasers performances [14–24]. Nevertheless, Nd^{3+} is not an ideal dopant for solar-pumped lasers due to the low spectral overlap of the Nd^{3+} absorption

spectrum with the blackbody-like solar emission spectrum, imposing limits to the efficiency of solar-powered lasers.

Co-doping the Nd:YAG medium with chromium (Cr^{3+}) or cerium (Ce^{3+}) ions may improve the solar laser efficiency by supplying a broader absorption band to overlap with the solar emission spectrum, when compared to simple Nd:YAG lasers [29–32]. The attempts to meliorate the solar laser efficiency using Cr:Nd:YAG have been carried out since 2007 [22–24]. The record in solar laser slope efficiency, obtained by measuring the laser output power variation with the incoming solar power, is 6.7%, reached in 2018 by end-side-pumping a Cr(0.1 at.%):Nd(1.0 at.%):YAG rod through a primary parabolic concentrator [24]. This result is 1.28 times more than the highest slope efficiency obtained by Nd:YAG laser rod end-side-pumped through a similar solar facility [16].

The mechanisms of energy transfer between Ce^{3+} and Nd^{3+} ions have also been studied for some time using dye lasers [33], lamps [34–36], LEDs [37], and laser diodes [38] as pumping sources. Still, the experimental evaluation of the Ce:Nd:YAG performance under broadband solar pumping is in its early stages [25–27]. The first solar laser experiment using a Ce:Nd:YAG laser medium was performed in 2020, by end-side-pumping a Ce(0.05 at.%):Nd(1.0 at.%):YAG rod of 5 mm in diameter and 30 mm in length at the medium size solar furnace (MSSF) of PROMES-CNRS [25]. The Ce:Nd:YAG rod emitted a 6.0 W cw laser power at an incoming solar power of 964 W. However, at higher solar power levels, the Ce:Nd:YAG laser power dropped abruptly, followed by a fracture of the laser rod in its upper-end region, where most of the solar rays were focused [25]. To try to minimize this problem, side-pumping configurations were adopted in the most recent Ce:Nd:YAG solar lasers [26,27]. Side-pumping is suitable for laser power scaling since it spreads the concentrated solar energy along the laser rod axis, minimizing the thermal load problems. For 1125 W of incoming solar power at the MSSF of PROMES-CNRS, the maximum cw solar laser power of 19.6 W was emitted by a side-pumped 4 mm diameter and 35 mm length Ce(0.1 at.%):Nd(1.1 at.%):YAG laser rod [27], corresponding to an increase of 3.27 times in relation to that of the previous end-side-pumped Ce:Nd:YAG solar laser through the same solar facility [25]. For efficient side-pumping of the Ce:Nd:YAG laser rod, a fused silica aspherical lens was used as a secondary concentrator [27]. However, this resulted in an uneven light distribution along the laser rod, which led to its fracture when adding more incoming solar power.

To scale the Ce:Nd:YAG solar laser to higher power levels, a uniformly pumped laser rod is extremely important. The use of side-pumping configurations employing fused silica light guides with a rectangular cross-section has allowed a substantial reduction of the thermal load and stress problems in either Nd:YAG or Cr:Nd:YAG laser rods [20–22]. Based on the principles of total internal reflection, the rectangular light guides shaped the near-Gaussian distribution of the concentrated sunlight spot incident on its input aperture into a homogeneous light distribution at its output aperture [20–22]. Consequently, the solar radiation was uniformly spread along the laser rod, significantly reducing the accumulated heat within the laser medium compared to previous solar lasers with no light guide [16,24–27]. The highest laser output power attained by side-pumping a laser rod with a light guide was 33.6 W, from a Cr:Nd:YAG laser rod of 7 mm in diameter and 30 mm in length, pumped through the 2 m diameter MSSF parabolic mirror [22].

Due to the abovementioned reasons, we decided to test the laser power scalability of a 4 mm diameter, 35 mm length Ce(0.1 at.%):Nd(1.1 at.%):YAG laser rod side-pumped by a rectangular fused silica light guide. The experiments were realized at the MSSF of PROMES-CNRS. The side-pumping configuration with the fused silica light guide allowed the Ce:Nd:YAG laser rod to withstand an elevated incoming solar power level of 2.6 kW, producing a 40 W cw solar laser power with the full collection area of the MSSF parabolic mirror. This, as far as we are aware, was the highest reported cw solar laser power emitted from a Ce:Nd:YAG solar laser medium. It was also the highest cw solar laser power achieved with side-pumping configuration using a light homogenizer.

2. Energy Transfer Mechanism of Ce^{3+} to Nd^{3+} in Ce:Nd:YAG Medium

Although reports on solar laser using Ce:Nd:YAG as a gain medium have appeared only recently [25–27], the effect of co-doping the Nd:YAG medium with Ce^{3+} ions has stimulated already decades of research [33–38]. The strong and broad absorption bands of Ce:Nd:YAG make this active material a suitable candidate for broadband pumped lasers. As observed in Figure 1, the absorption spectrum of Ce:Nd:YAG presents two broad bands characteristic of the Ce^{3+} ion in a YAG lattice, which are centered at 339 nm and 460 nm (Figure 1b) and overlap well with the solar spectrum region of greater intensity (Figure 1a). It has also other bands in the red and near infrared (NIR) regions that are characteristic of the Nd^{3+} ions (Figure 1c).

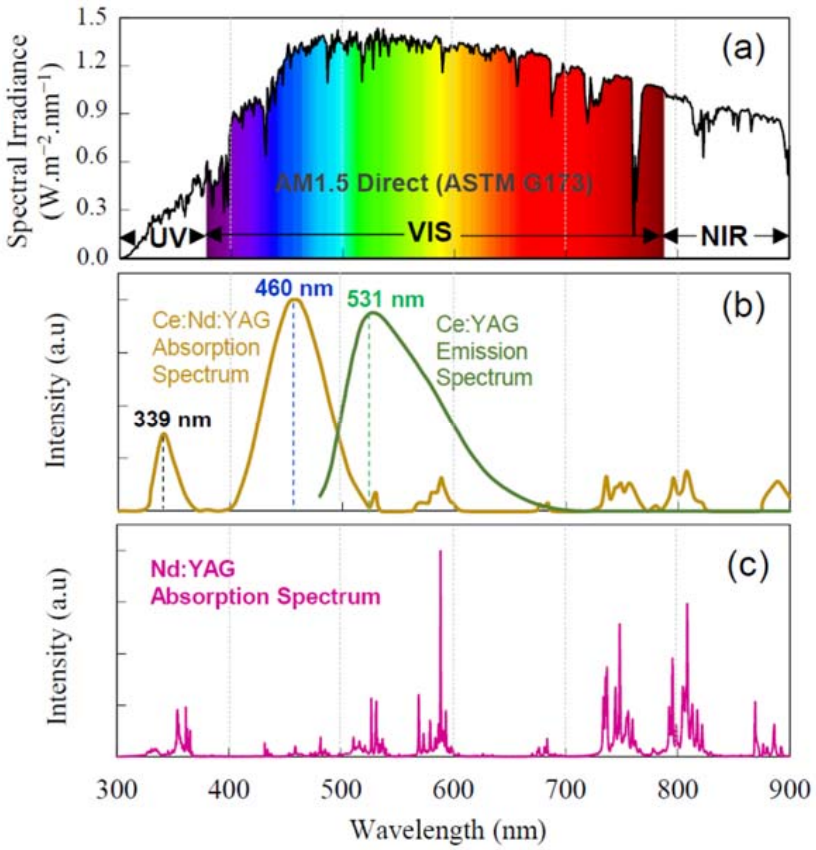

Figure 1. (**a**) AM1.5 direct solar spectrum at 300–900 nm wavelength range, adapted from [39]; UV, ultraviolet; VIS, visible; NIR, near infrared; (**b**) Ce:Nd:YAG absorption spectrum and Ce:YAG fluorescence spectrum, adapted from [35,40], respectively; (**c**) Nd:YAG absorption spectrum, adapted from [41].

Figure 2 illustrates the energy level diagram of Ce:Nd:YAG and the transfer mechanism between the Ce^{3+} and Nd^{3+} ions. When pumping Ce:Nd:YAG with broadband radiation, with wavelengths centered around 339 nm and 460 nm, the Ce^{3+} ions are excited from the $^2F_{5/2}$ ground state level to the pump bands of $5d_2$ ($^2B_{1g}$) and $5d_1$ ($^2A_{1g}$), respectively. The excited electrons in the $5d_2$ ($^2B_{1g}$) pump band then relax non-radiatively (dashed black line) to the lower $5d_1$ pump band and further decay radiatively to the $^2F_{5/2}$ ground state (solid green line). Since the absorption spectrum of Ce:Nd:YAG is quite broad, a strong and broad emission luminescence centered at 531 nm occurs (Figure 1b), which overlaps with the strong peak absorptions of Nd^{3+} in the green and yellow spectral region (Figure 1c). Therefore, a radiative transfer mechanism takes place between the $5d_1(^2A_{1g}) \rightarrow {}^2F_{5/2}$ and $^4I_{9/2} \rightarrow {}^2G_{7/2}$ transitions of Ce^{3+} and Nd^{3+} ions, respectively, through a cross-relaxation process [33–35,38], as indicated by the pathway (1) of Figure 2.

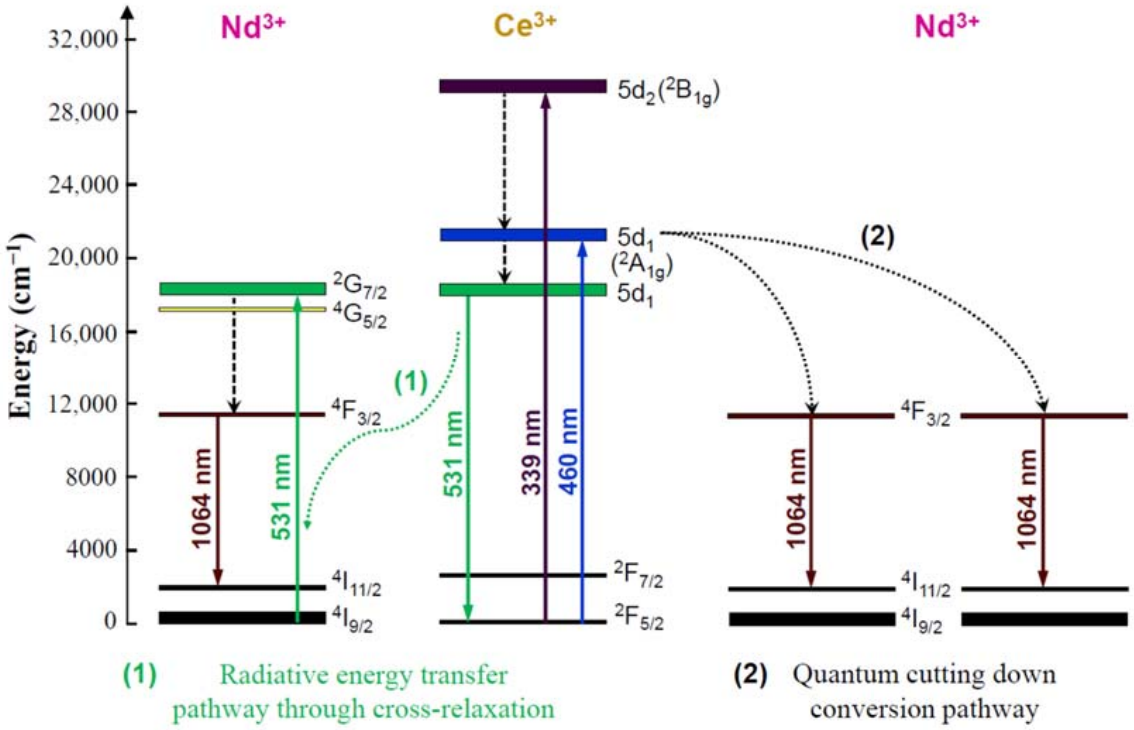

Figure 2. Energy-level diagram representing the energy transfer between Ce^{3+} and Nd^{3+} ions in the Ce:Nd:YAG material, adapted from [35]. (**1**) Radiative energy transfer pathway through cross-relaxation; (**2**) Quantum cutting down conversion pathway.

Another energy transfer mechanism may also occur, based on a quantum cutting down-conversion process [35,42], as represented by pathway (2). This process implies that two NIR photons could emit from one absorbed visible (VIS) photon. Its occurrence is possible in Ce:Nd:YAG due to the excitation of Ce^{3+} to the higher $5d_1(^2A_{1g})$ energy level, whose transition to the $^2F_{5/2}$ ground-state level has approximately twice the energy difference between the $^4F_{3/2}$ and $^4I_{11/2}$ levels of the Nd^{3+}.

3. Description of the Ce:Nd:YAG Solar Laser System

3.1. Medium Size Solar Furnace of the PROMES-CNRS

The solar facility is constituted by a heliostat and a stationary parabolic concentrator with horizontal axis. The heliostat has 36 flat mirror segments, each with 0.5 m × 0.5 m dimensions, which tracks and redirects the solar rays to the parabolic mirror with a 2.0 m diameter, a 0.85 m focal distance, and a 60° rim angle [16,20–22,25], as illustrated in Figure 3a. Both heliostat and parabolic mirrors are back-silvered, each with less than 80% reflectivity due to iron contents in the glass substrate and degradation owing to many years of usage. Hence, about 59% of the incoming solar rays are focused [16,21,22,25], reaching a maximum of 2 kW of power at the focus [43].

For the solar laser experiments, the Ce:Nd:YAG solar laser head, along with the resonant cavity, was fixed on a mechanical support with automatic X-Y-Z axis calibration at the focal zone of the MSSF, as shown in Figure 3b. The incoming solar power was regulated by a shutter with motorized blades. When the shutter was totally open, a 2.48 m^2 effective collection area was measured for the maximum diameter of the parabolic mirror. All the shadow effects in the MSSF caused by the space between the flat mirrors of the heliostat, the shutter blades, the laser head, and respective mechanical supports, have been accounted for.

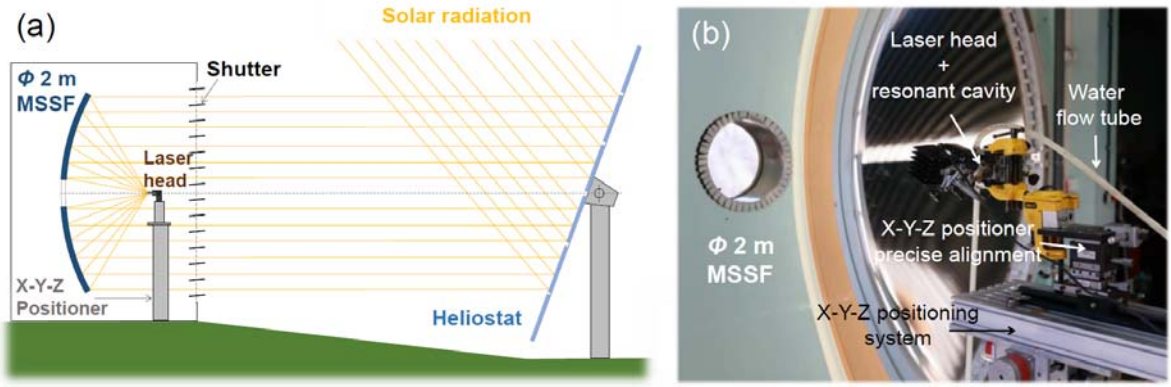

Figure 3. (**a**) Design of the PROMES-CNRS solar facility. (**b**) Photograph of the Medium Size Solar Furnace (MSSF) and the solar laser head mounting.

3.2. Side-Pumped Solar Laser Head with the Fused Silica Homogenizer

A schematic design of the laser head is given in Figure 4. It is composed of a rectangular fused silica light guide and a two-dimensional (2D) V-shaped pump cavity, within which the Ce:Nd:YAG laser rod was fixed, being actively cooled by water.

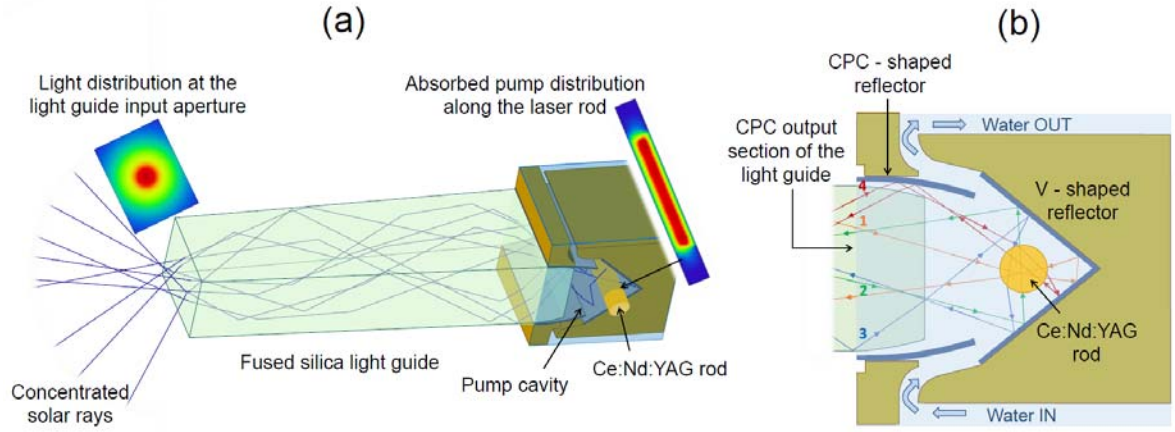

Figure 4. Schematic designs of (**a**) the Ce:Nd:YAG solar laser head with rectangular light guide and (**b**) the V-shaped pump cavity with the passage of pump rays within the laser rod. The insets of (**a**) represent the solar rays' distribution at both the light guide input aperture (**left**) and along the laser rod (**right**).

Fused silica material is suitable for solar-powered lasers since it has a wide transparency range over the Ce:Nd:YAG absorption spectrum. Furthermore, it is very resistant to high temperature and thermal shock [44]. The light guide with a 14 mm × 18.4 mm input aperture collected the MSSF-concentrated solar radiation with a near-Gaussian profile of 11 mm full width at half maximum [16,21,25]. The solar rays were then internally reflected along a 68 mm length of the light guide, to its 2D compound parabolic concentrator (CPC) output section with 12 mm × 22 mm output aperture and 5.5 mm length. As demonstrated in Figure 4a, the fused silica light guide behaves like a beam homogenizer, enabling a homogeneous absorbed pump light distribution along the Ce:Nd:YAG laser rod. This helps not only to reduce the thermal effects in the laser rod, but also to compensate the heliostat tracking error-dependent losses [20–22], leading to higher solar laser beam stability compared to solar lasers with no light homogenizer [45].

To produce the light guide, a fused silica slab of 99.995% optical purity with 14 mm × 22 mm × 75 mm dimensions (supplied by Beijing Aomolin Ltd., Bejing, China), was ground and polished to the final dimensions abovementioned. The side surfaces of the light guide were slightly inclined to ensure its easy mechanical attachment to the laser

head. The 2D-CPC sidewalls of the light guide provided effective coupling of the solar rays to the laser rod. It is also worth noting that the direct cooling of the laser rod with water is of utmost importance to prevent the laser rod from UV and IR heating. A water flow rate of about 6 L/min was adopted in the present work, which was essential to dissipate the heat within the laser head.

The water-flooded V-shaped pump cavity had a 10 mm depth and a 16 mm × 22 mm entrance aperture, positioned at the exit of the 2D CPC-shaped upper reflectors with a 12 mm × 22 mm output aperture. This arrangement provided the zigzag path of the solar rays within the Ce:Nd:YAG laser rod. As demonstrated in Figure 4b, ray one (orange color) hits directly the laser medium and is redirected back to the rod by the V-shaped cavity so that double-pass pumping is accomplished. The solar rays from the light guide that do not directly reach the laser rod, represented by rays two (green color) and three (blue color), can be redirected again to the laser rod by the V-shaped reflector. The upper 2D CPC-shaped reflectors also help to redirect the rays that exit the 2D CPC surface of the light-guide to the laser rod, as demonstrated by the optical path of ray four (red color), which may pass through the rod twice with the help of the V-shaped cavity. The inner walls of the V-shaped section, as well as the upper part section of the pump cavity, were covered with silver-coated aluminum foils of 94% reflectivity.

A high reflection (HR) coated mirror (99.9% @ 1064 nm), the Ce:Nd:YAG laser rod, and a partial reflection (PR) coated mirror (R $\geq$ 95 $\pm$ 2% @ 1064 nm) formed the optical resonator, as shown in Figure 5. The 4 mm diameter and 35 mm length Ce(0.1 at.%):Nd(1.1 at.%):YAG rod was manufactured by Chengdu Dongjun Laser Co., Ltd. The end faces of the laser rod were covered with anti-reflective coating for 1064 nm (reflectivity (R) < 0.2% @ 1064 nm). Both HR and PR laser mirrors were supplied by ESKMA Optics.

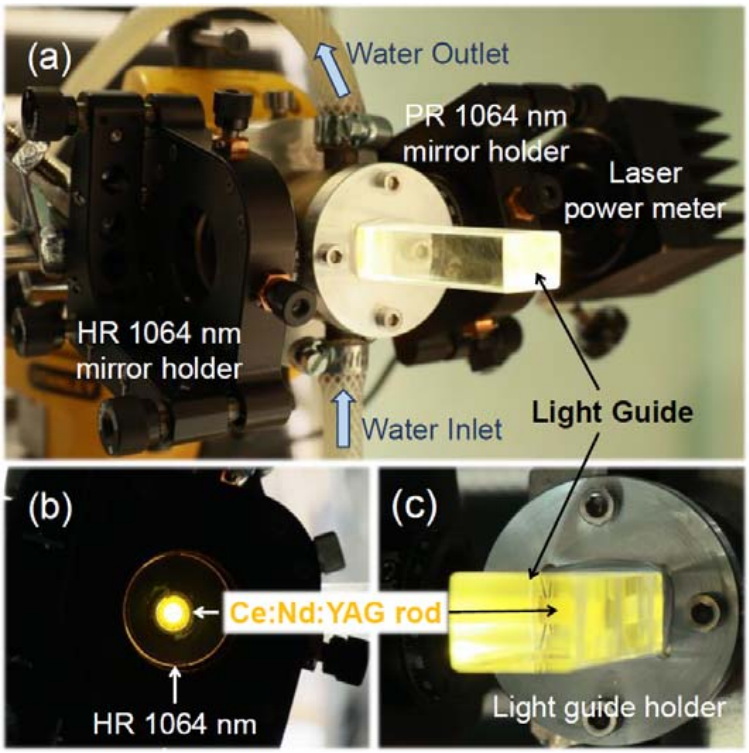

Figure 5. Photograph of (**a**) the Ce:Nd:YAG solar-pumped laser head with the laser resonator and (**b**,**c**) the detailed view of the Ce:Nd:YAG laser medium in the experiments. HR, high reflection; PR, partial reflection.

The present scheme was designed and produced in Lisbon. It was then tested at the 2 m diameter MSSF of the PROMES-CNRS, during the winter period of February 2022.

4. Solar-Pumped Ce:Nd:YAG Laser Experiments with the Rectangular Fused Silica Light Guide

To examine the Ce:Nd:YAG medium resistance under extreme solar pumping and, hence, its aptitude to scale to higher power levels, the performance of the Ce:Nd:YAG solar laser was evaluated as a function of the MSSF diameter D, starting from relatively small (D = 1.38 m) to the maximum diameter of the MSSF (D = 2.0 m). For maximum laser power extraction from the active medium in each case, the HR and PR laser mirrors were optically aligned as close as possible to the laser rod, as shown in Figure 5, forming a short and symmetric laser resonator with a 60 mm total length. Therefore, the Ce:Nd:YAG solar laser operated in a multimode regime. Flat laser mirrors were used to provide less laser beam divergence in relation to that with concave laser mirrors.

The influence of the incoming solar power on the Ce:Nd:YAG solar laser output power with four different Ds (1.38 m; 1.60 m; 1.78 m; 2.0 m) is given in Figure 6. During the experiments, the solar irradiances varied from 1000 to 1060 W/m^2, measured with a Kipp & Zonen CH1 pyrheliometer on a Kipp & Zonen 2AP solar tracker. Laser output power measurements were registered with a PM1100D power meter from Thorlabs.

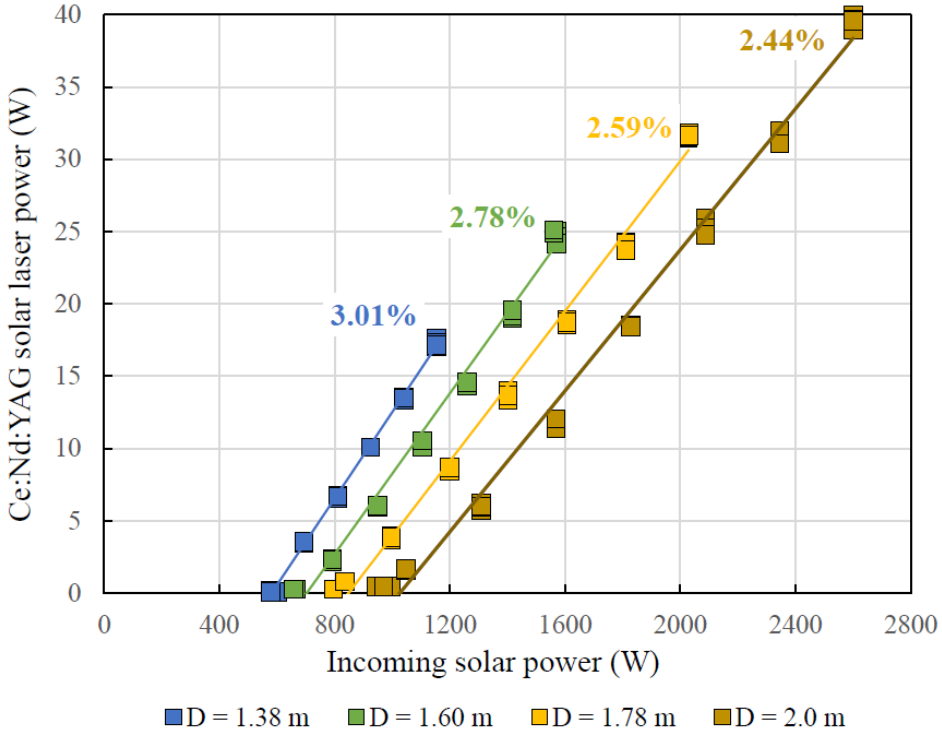

Figure 6. Variation of the Ce:Nd:YAG solar laser power with the incoming solar power and parabolic mirror diameter (D).

Table 1 summarizes the performance of the Ce:Nd:YAG solar laser output at each case, in terms of threshold solar power, maximum laser power, and slope efficiency. The M^2 beam quality factors for D = 1.38 m and D = 2.0 m are also given. Near-circular laser beam profiles and high evaporation rates were observed on an opaque material, placed at a distance of 1 m from the PR output mirror.

As observed in Figure 6, the variation of the solar concentrator diameter strongly influenced the laser performance of the Ce:Nd:YAG medium. It performed better with a lower D = 1.38 m, started to emit a laser at a minimum incoming solar power of 578 W, and reached a laser output power of 17.4 W at an incoming solar power of 1154 W. The slope efficiency of 3.01% was hence calculated in this case. $M^2_x \approx M^2_y \approx 38$ laser beam quality factors were also registered with D = 1.38 m. These results were slightly worse than that of the most recent Ce:Nd:YAG laser rod with a fused silica aspherical lens as a secondary concentrator, tested under similar pumping conditions, through which a 19.6 W cw laser

power and 3.03% slope efficiency were measured [27]. The use of the aspheric lens helped to preserve the concentrated solar radiation profile, thus allowing to a certain extent a more effective side-pumping of the laser rod. However, at incoming solar powers greater than 1125 W, the non-uniformity of the absorption profile of the Ce:Nd:YAG laser rod led to its fracture [27], which means that the laser rod could not withstand more than 43% of the total incoming solar power of the MSSF. On the contrary, with the use of the light guide as a secondary concentrator, the Ce:Nd:YAG solar laser remained operational even with the maximum collection area of the MSSF, as shown in both Figure 6 and Table 1. Despite the decrease in slope efficiency to 2.44% and the deterioration of the laser beam quality to $M^2_x \approx 52$, $M^2_y \approx 54$ factors with an increasing collection area, a 40 W cw solar laser output power was reached for D = 2 m, without damaging the Ce:Nd:YAG laser rod. This was the highest laser power achieved with the Ce:Nd:YAG laser medium pumped by broadband solar radiation, being twice that obtained by the previous side-pumped Ce:Nd:YAG solar laser [27]. It was also 1.19 times more than the maximum solar laser power emitted from a side-pumped Cr:Nd:YAG laser rod using light guide [22].

Table 1. Ce:Nd:YAG solar laser performance with light guide with different parabolic mirror diameters (D).

Collection Diameter, D	D = 1.38 m	D = 1.60 m	D = 1.78 m	D = 2.00 m
Rim angle, α	44°	50°	55°	60°
Effective collection area	1.09 m^2	1.53 m^2	1.93 m^2	2.48 m^2
Maximum incoming solar power	1154 W	1559 W	2033 W	2600 W
Minimum threshold solar power	578 W	657 W	795 W	943 W
Maximum laser output power	17.35 W	25.13 W	31.80 W	40.01 W
Slope efficiency	3.01%	2.78%	2.59%	2.44%
M^2_x, M^2_y factors	38, 38	—	—	52, 54

5. Conclusions

The potential of the Ce:Nd:YAG laser medium for solar laser power scaling was evaluated at the MSSF of PROMES-CNRS. The adoption of the side-pumping configuration with a rectangular light guide ensured a uniform pump light distribution along the laser rod. Thanks to this, the 4 mm diameter and 35 mm length Ce(0.1 at.%):Nd(1.1 at.%):YAG rod demonstrated a remarkable resistance to highly incoming solar powers, compared to the previous Ce:Nd:YAG solar lasers [25,27]. By using the total incoming solar power of the MSSF, a 40 W cw solar laser power was registered. As far as we are aware, this was the highest laser power level reported from a solar powered Ce:Nd:YAG laser medium, being two times more than that from the most recent Ce:Nd:YAG laser rod side-pumped with an aspheric lens secondary concentrator at the MSSF [27]. It was also the highest side-pumped solar laser power through light guide [20–22]. Therefore, the side-pumping of the laser rod, with the help of the fused silica light homogenizer, proved to be a good solution for scaling the solar laser power with the Ce:Nd:YAG laser medium.

In future work, either side-pumping or end-side-pumping configurations with light-guides could be employed for the simultaneous pumping of several Ce:Nd:YAG laser rods of smaller diameters within a common pumping cavity. The highly concentrated solar radiation could hence be evenly shared by the several laser rods, ensuring not only a substantial alleviation of the thermal lensing effects in solar-powered lasers [19], but also a significant rise in solar laser conversion efficiency. This may pave the way of Ce:Nd:YAG solar laser research into a new phase of development in terms of efficiency, laser beam quality, and stability at higher power levels.

Author Contributions: Conceptualization, J.A. and D.L.; methodology, J.A. and D.L.; validation, J.A., D.L. and C.R.V.; formal analysis, J.A., D.L. and C.R.V.; investigation, J.A., D.L., C.R.V., D.G. and E.G.; resources, D.L., J.A. and E.G.; data curation, J.A., C.R.V., D.L., D.G., B.D.T., H.C. and M.C.; writing—original draft preparation, J.A.; writing—review and editing, J.A., D.L., D.G., B.D.T., H.C.,

M.C. and C.R.V.; supervision, D.L.; project administration, D.L.; funding acquisition, D.L., J.A. and E.G. All authors have read and agreed to the published version of the manuscript.

Funding: This research was financially supported by Science and Technology Foundation of Portuguese Ministry of Science, Technology and Higher Education (FCT-MCTES) in the framework of the strategic project UIDB/00068/2020 and the exploratory research project EXPL/FIS-OTI/0332/2021. The solar laser research was also supported by the Solar Facilities for European Research Area–Third Phase (SFERA III), Grant Agreement No. 823802.

Institutional Review Board Statement: Not applicable.

Informed Consent Statement: Not applicable.

Data Availability Statement: Not applicable.

Acknowledgments: The authors express their gratitude for the FCT-MCTES fellowship grants CEECIND/03081/2017, PD/BD/142827/2018, PD/BD/128267/2016, 2021.06172.BD, SFRH/BD/145322/2019 and SFRH/BPD/125116/2016.

Conflicts of Interest: The authors declare no conflict of interest.

References

1. The Global Goals, Goal 7: Affordable and Clean Energy. Available online: https://www.globalgoals.org/goals/7-affordable-and-clean-energy/ (accessed on 1 April 2022).
2. The Global Goals, Goal 9: Industry, Innovation and Infrastructure. Available online: https://www.globalgoals.org/goals/9-industry-innovation-and-infrastructure/ (accessed on 1 April 2022).
3. Yabe, T.; Bagheri, B.; Ohkubo, T.; Uchida, S.; Yoshida, K.; Funatsu, T.; Oishi, T.; Daito, K.; Ishioka, M.; Yasunaga, N.; et al. 100 W-class solar pumped laser for sustainable magnesium-hydrogen energy cycle. *J. Appl. Phys.* **2008**, *104*, 083104. [CrossRef]
4. Motohiro, T.; Takeda, Y.; Ito, H.; Hasegawa, K.; Ikesue, A.; Ichikawa, T.; Higuchi, K.; Ichiki, A.; Mizuno, S.; Ito, T.; et al. Concept of the solar-pumped laser-photovoltaics combined system and its application to laser beam power feeding to electric vehicles. *Jpn. J. Appl. Phys.* **2017**, *56*, 08MA07. [CrossRef]
5. Abdel-Hadi, Y.A. Space-based solar laser system simulation to transfer power onto the earth. *NRIAG J. Astron. Geophys.* **2020**, *9*, 558–562. [CrossRef]
6. Weaver, W.R.; Lee, J.H. A Solar Pumped Gas Laser for the Direct Conversion of Solar Energy. *J. Energy* **1983**, *7*, 498–501. [CrossRef]
7. Kiss, Z.J.; Lewis, H.R.; Duncan, R.C. Sun pumped continuous optical maser. *Appl. Phys. Lett.* **1963**, *2*, 93–94. [CrossRef]
8. Insuik, R.J.; Christiansen, W.H. Blackbody-pumped CO_2 laser experiment. *AIAA J.* **1984**, *22*, 1271–1274. [CrossRef]
9. Terry, C.K.; Peterson, J.E.; Goswami, D.Y. Terrestrial solar-pumped iodine gas laser with minimum threshold concentration requirements. *J. Thermophys. Heat Transf.* **1996**, *10*, 54–59. [CrossRef]
10. Lee, J.H.; Kim, K.C.; Kim, K.H. Threshold pump power of a solar-pumped dye laser. *Appl. Phys. Lett.* **1988**, *53*, 2021–2022. [CrossRef]
11. Arashi, H.; Oka, Y.; Sasahara, N.; Kaimai, A.; Ishigame, M. A Solar-Pumped cw 18 W Nd:YAG Laser. *Jpn. J. Appl. Phys.* **1984**, *23*, 1051–1053. [CrossRef]
12. Weksler, M.; Shwartz, J. Solar-pumped solid-state lasers. *IEEE J. Quantum Electron.* **1988**, *24*, 1222–1228. [CrossRef]
13. Lando, M.; Kagan, J.; Linyekin, B.; Dobrusin, V. A solar-pumped Nd:YAG laser in the high collection efficiency regime. *Opt. Commun.* **2003**, *222*, 371–381. [CrossRef]
14. Dinh, T.H.; Ohkubo, T.; Yabe, T.; Kuboyama, H.J.O.L. 120 watt continuous wave solar-pumped laser with a liquid light-guide lens and an Nd:YAG rod. *Opt. Lett.* **2012**, *37*, 2670–2672. [CrossRef] [PubMed]
15. Liang, D.; Almeida, J. Highly efficient solar-pumped Nd:YAG laser. *Opt. Express* **2011**, *19*, 26399–26405. [CrossRef] [PubMed]
16. Liang, D.; Almeida, J.; Vistas, C.R.; Guillot, E. Solar-pumped Nd:YAG laser with 31.5W/m^2 multimode and 7.9W/m^2 TEM_{00}-mode collection efficiencies. *Sol. Energy Mater. Sol. Cells* **2017**, *159*, 435–439. [CrossRef]
17. Guan, Z.; Zhao, C.; Li, J.; He, D.; Zhang, H. 32.1 W/m^2 continuous wave solar-pumped laser with a bonding Nd:YAG/YAG rod and a Fresnel lens. *Opt. Laser Technol.* **2018**, *107*, 158–161. [CrossRef]
18. Guan, Z.; Zhao, C.; Zhang, H.; Li, J.; He, D.; Almeida, J.; Vistas, C.R.; Liang, D. 5.04% system slope efficiency solar-pumped Nd:YAG laser by a heliostat-parabolic mirror system. *J. Photonics Energy* **2018**, *8*, 2. [CrossRef]
19. Liang, D.; Almeida, J.; Garcia, D.; Tibúrcio, B.D.; Guillot, E.; Vistas, C.R. Simultaneous solar laser emissions from three Nd:YAG rods within a single pump cavity. *Sol. Energy* **2020**, *199*, 192–197. [CrossRef]
20. Almeida, J.; Liang, D.; Guillot, E. Improvement in solar-pumped Nd:YAG laser beam brightness. *Opt. Laser Technol.* **2012**, *44*, 2115–2119. [CrossRef]
21. Almeida, J.; Liang, D.; Vistas, C.R.; Bouadjemine, R.; Guillot, E. 5.5 W continuous-wave TEM_{00}-mode Nd:YAG solar laser by a light-guide/2V-shaped pump cavity. *Appl. Phys. B* **2015**, *121*, 473–482. [CrossRef]

22. Liang, D.; Almeida, J.; Guillot, E. Side-pumped continuous-wave Cr:Nd:YAG ceramic solar laser. *Appl. Phys. B Lasers Opt.* **2013**, *111*, 305–311. [CrossRef]
23. Yabe, T.; Ohkubo, T.; Uchida, S.; Yoshida, K.; Nakatsuka, M.; Funatsu, T.; Mabuti, A.; Oyama, A.; Nakagawa, K.; Oishi, T.; et al. High-efficiency and economical solar-energy-pumped laser with Fresnel lens and chromium codoped laser medium. *Appl. Phys. Lett.* **2007**, *90*, 261120. [CrossRef]
24. Liang, D.; Vistas, C.R.; Tibúrcio, B.D.; Almeida, J. Solar-pumped Cr:Nd:YAG ceramic laser with 6.7% slope efficiency. *Sol. Energy Mater. Sol. Cells* **2018**, *185*, 75–79. [CrossRef]
25. Vistas, C.R.; Liang, D.; Garcia, D.; Almeida, J.; Tibúrcio, B.D.; Guillot, E. Ce:Nd:YAG continuous-wave solar-pumped laser. *Optik* **2020**, *207*, 163795. [CrossRef]
26. Vistas, C.; Liang, D.; Almeida, J.; Tibúrcio, B.; Garcia, D.; Catela, M.; Costa, H.; Guillot, E. Ce:Nd:YAG side-pumped solar laser. *J. Photonics Energy* **2021**, *11*, 018001. [CrossRef]
27. Vistas, C.R.; Liang, D.; Garcia, D.; Catela, M.; Tibúrcio, B.D.; Costa, H.; Guillot, E.; Almeida, J. Uniform and Non-Uniform Pumping Effect on Ce:Nd:YAG Side-Pumped Solar Laser Output Performance. *Energies* **2022**, *15*, 3577. [CrossRef]
28. Lupei, V.; Lupei, A.; Gheorghe, C.; Ikesue, A. Emission sensitization processes involving Nd^{3+} in YAG. *J. Lumin.* **2016**, *170*, 594–601. [CrossRef]
29. Saiki, T.; Uchida, S.; Imasaki, K.; Motokoshi, S.; Yamanaka, C.; Fujita, H.; Nakatsuka, M.; Izawa, Y. Oscillation Property of Disk-Type Nd/Cr:YAG Ceramic Lasers with Quasi-Solar Pumping, (CLEO). In Proceedings of the Lasers and Electro-Optics, Baltimore, MD, USA, 22–27 May 2005; Volume 2, pp. 915–917.
30. Yagi, H.; Yanagitani, T.; Yoshida, H.; Nakatsuka, M.; Ueda, K. The optical properties and laser characteristics of Cr^{3+} and Nd^{3+} co-doped $Y_3Al_5O_{12}$ ceramics. *Opt. Laser Technol.* **2007**, *39*, 1295–1300. [CrossRef]
31. Payziyev, S.; Makhmudov, K.; Abdel-Hadi, Y.A. Simulation of a new solar Ce:Nd:YAG laser system. *Optik* **2018**, *156*, 891–895. [CrossRef]
32. Payziyev, S.; Sherniyozov, A.; Bakhramov, S.; Zikrillayev, K.; Khalikov, G.; Makhmudov, K.; Ismailov, M.; Payziyeva, D. Luminescence sensitization properties of Ce:Nd:YAG materials for solar pumped lasers. *Opt. Commun.* **2021**, *499*, 127283. [CrossRef]
33. Mares, J.; Jacquier, B.; Pédrini, C.; Boulon, G.J.R.P.A. Energy transfer mechanisms between Ce^{3+} and Nd^{3+} in YAG: Nd, Ce at low temperature. *Rev. Phys. Appliquée* **1987**, *22*, 145–152. [CrossRef]
34. Meng, J.X.; Li, J.Q.; Shi, Z.P.; Cheah, K.W. Efficient energy transfer for Ce to Nd in Nd/Ce codoped yttrium aluminum garnet. *Appl. Phys. Lett.* **2008**, *93*, 221908. [CrossRef]
35. Tai, Y.; Zheng, G.; Wang, H.; Bai, J. Near-infrared quantum cutting of Ce^{3+}–Nd^{3+} co-doped $Y_3Al_5O_{12}$ crystal for crystalline silicon solar cells. *J. Photochem. Photobiol. A Chem.* **2015**, *303–304*, 80–85. [CrossRef]
36. Guo, Y.; Huang, J.; Ke, G.; Ma, Y.; Quan, J.; Yi, G. Growth and optical properties of the Nd,Ce:YAG laser crystal. *J. Lumin.* **2021**, *236*, 118134. [CrossRef]
37. Villars, B.; Steven Hill, E.; Durfee, C.G. Design and development of a high-power LED-pumped Ce:Nd:YAG laser. *Opt. Lett.* **2015**, *40*, 3049–3052. [CrossRef] [PubMed]
38. Samuel, P.; Yanagitani, T.; Yagi, H.; Nakao, H.; Ueda, K.I.; Babu, S.M. Efficient energy transfer between Ce^{3+} and Nd^{3+} in cerium codoped Nd: YAG laser quality transparent ceramics. *J. Alloys Compd.* **2010**, *507*, 475–478. [CrossRef]
39. *ASTM G173-03*; Standard Tables for Reference Solar Spectral Irradiances: Direct Normal and Hemispherical on 37° Tilted Surface. ASTM International: West Conshohocken, PA, USA, 2012.
40. Nishiura, S.; Tanabe, S.; Fujioka, K.; Fujimoto, Y. Properties of transparent Ce: YAG ceramic phosphors for white LED. *Opt. Mater.* **2011**, *33*, 688–691. [CrossRef]
41. Prahl, S. Nd:YAG—Nd:Y3Al5O12. Available online: https://omlc.org/spectra/lasermedia/html/052.html (accessed on 1 April 2022).
42. Liu, X.; Teng, Y.; Zhuang, Y.; Xie, J.; Qiao, Y.; Dong, G.; Chen, D.; Qiu, J. Broadband conversion of visible light to near-infrared emission by Ce^{3+}, Yb^{3+}-codoped yttrium aluminum garnet. *Opt. Lett.* **2009**, *34*, 3565–3567. [CrossRef]
43. PROMES-CNRS Solar Furnaces and Concentrating Solar Systems. Available online: https://www.promes.cnrs.fr/en/infrastructure-solaire/moyens-solaires/solar-furnaces-and-concentrating-solar-systems/ (accessed on 1 April 2022).
44. Heraeus Properties of Fused Silica. Available online: https://www.heraeus.com/en/hca/fused_silica_quartz_knowledge_base_1/properties_1/properties_hca.html (accessed on 1 April 2022).
45. Mehellou, S.; Liang, D.; Almeida, J.; Bouadjemine, R.; Vistas, C.R.; Guillot, E.; Rehouma, F. Stable solar-pumped TEM_{00}-mode 1064 nm laser emission by a monolithic fused silica twisted light guide. *Sol. Energy* **2017**, *155*, 1059–1071. [CrossRef]